Constraining Dark Matter Density in the Galactic Center Using the Peribothron Shift in the Orbit of S2

(PHYSICS/ASTRONOMY)

Author: Devi Kuscer
School: United World College of the Atlantic
Llantwit Major, Wales
Pioneer Research Concentration: Relativity and Cosmology

Constraining Dark Matter Density in the Galactic Center Using the Peribothron Shift of the Orbit of S2

Devi Kuscer

Author background: *Devi Kuscer grew up in Slovenia and the UK and currently attends United World College Atlantic in Wales, United Kingdom. Her Pioneer concentration was in the field of Physics and titled Cosmology, Relativity and the Contents of the Universe.*

Abstract

In this paper, we first find the parameters of the precessing orbit of S2, a main sequence B-type star orbiting the black hole Sagittarius A*, including the semi-major axis, the eccentricity, and the angle of rotation, along with their associated uncertainties. We then use the method of adding a correction term to the central potential relating to the Plummer potential, to derive the equations of motions for an orbit containing a perturbation due to the presence of an additional dark matter mass. From the obtained equations of motion we then find the solution for the classical Newtonian orbit as well as the perturbed orbit. Knowing the Peribothron shift and other parameters, we are able to solve for $M_{DM}a^2$ where M_{DM} is the mass of the dark matter and a is the radius of the central core of the dark matter halo. We then assume a value of $0.1kpc$ for a to find a function for dark matter density with respect to the distance from the central core and constrain the density of dark matter in the galactic center. From this we are able to find that the upper bound of the density of dark matter in the Milky Way galactic center to be approximately $2.83 \times 10^{-13} M_{\odot}/pc^3$.

1. Introduction

1.1. Dark Matter in the Galactic Center

Dark matter is speculated to account for around 27% of the contents of the universe; however, unlike ordinary matter, it does not absorb, emit, or detect light making it incredibly hard to detect.

One of the main pieces of evidence for the presence of dark matter in the galactic centers arises from the plateauing of galactic rotation curves. A rotation curve of a galaxy is a plot of the orbital velocity of stellar objects (v) against their distance from the galactic center (r)[1]. Conversely to Newton's law of gravity, which predicts that the rotational velocity should decrease with increased distance from the galactic center, when measured, the velocities of the outer-most regions of galaxies remain constant[2]. This means that the stars in the outermost regions of galaxies are moving faster than can be accounted for by ordinary matter and suggests that this phenomenon is being caused by a large

dark halo of unseen matter - dark matter[3]. This dark matter halo is speculated to be spherical and enshrouds the galaxy, providing the additional gravitational pull needed to cause a constant rotation curve. The dark matter distribution in galaxies influences their formation and evolution therefore studying the dark matter density of the galactic center could help us better understand galactic growth and stability.

1.2. The Plummer Profile for Dark Matter

The Plummer Profile describes a system that contains a central core of high density which then smoothly decreases with increased distance from the core[4]. The model was originally developed to describe the density distributions of star clusters; however, the Plummer potential is also used in N-body simulations[5] as it prevents the simulation from generating un-physically large forces during close encounters between bodies.

The Plummer potential is defined as[6]:

$$V(r) = -\frac{GM}{\sqrt{r^2 + a^2}} \tag{1}$$

This shows that instead of the gravitational potential becoming extremely large as r approaches 0, the additional correction introduced in the Plummer potential means that, as r approaches 0, the potential will approach a finite value.

It has also been used as a possible profile for the distribution of dark matter in the galactic halos enshrouding galaxies. This is because, unlike other profiles, the Plummer profile does not encounter the core/cusp problem where while computer simulations predict that dark matter density increases very steeply with decreased distance from the galactic center, observations show that the central density of dark matter remains constant in the central core rather than suddenly rising[7].

The formula for the density distribution in a Plummer profile system is defined as:

$$\rho(r) = \frac{3M}{4\pi a^3}\left(1 + \frac{r^2}{a^2}\right)^{\frac{-5}{2}} \tag{2}$$

where M is the mass of the system, a is the Plummer radius, which denotes the size of the central core, and r is the radial distance from the center of the central core. In this profile, when r approaches 0, the density does not diverge but instead flattens out, which creates a core with a constant density. This property makes the profile useful when analyzing dark matter systems, where the central density remains constant rather than forms a sharp cusp such as suggested by other models.

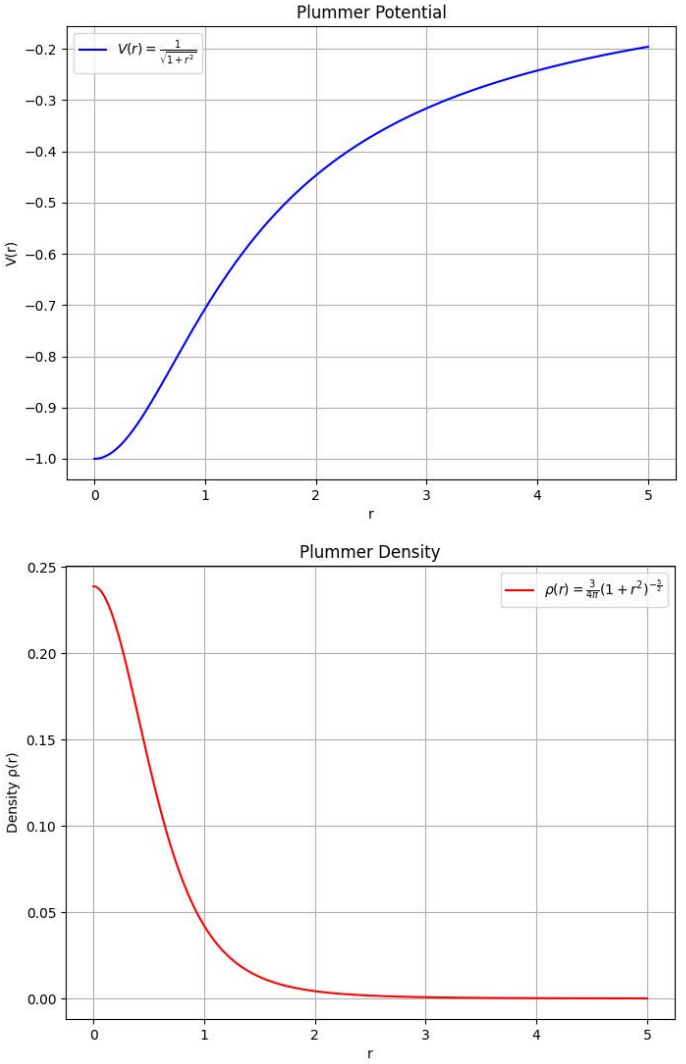

Figure 1*: General plot of Plummer potential and Plummer density.*

1.3. Peribothron Shift

The peribothron is the point of an orbit of a body that is closest to the black hole, it is in this way very similar to the perihelion which is defined as the point in the orbit of a planet, comet or asteroid which is closest to the Sun. A peribothron shift is therefore comparable to a perihelion shift which has been most famously observed in the orbit of Mercury.

In an ideal Newtonian orbit, where the system is only composed of a central and an orbiting body, the perihelion is expected to occur at the same point every orbit. However, the presence of other bodies, such as other planets orbiting the Sun in the

example of Mercury, causes a small advance in the perihelion which can be explained by the Newtonian gravitational theory by taking into account all of the perturbing forces brought on by the other orbiting bodies. However, the Newtonian gravitational theory fails to account for the entire perihelion advance. In the example of Mercury, it failed to account for 43″ of the total 5600″ of the perihelion shift. This inconsistency with Newtonian theory was first highlighted in 1859 by the French astrophysicist Urbain Le Verrier[8] and was attempted to be explained by the addition of a small planet, Vulcan, near Mercury; however, this attempt and many others were unsuccessful in explaining the precession of Mercury's orbit. Finally, it was Einstein who found a solution to the problem in 1916[9]. The additional perihelion shift can be explained by general relativity which states that due to the curvature of space-time caused by the central body, the perihelion of the orbiting body will precess more than what is explained only by Newton's law of gravitation. The perihelion advance due to general relativity ($\delta\phi_{gr}$) is given by the formula[10]:

$$\delta\phi_{gr} \approx \frac{3\pi r_g}{A(1-e^2)} \tag{3}$$

where r_g is the Schwarzschild radius, A is the semi-major axis of the orbit, and e is the eccentricity of the orbit. The Schwarzschild radius is also defined as: $r_g = \frac{2GM}{c^2}$ where G is Newton's gravitational constant, M is the mass of the body, and c is the speed of light. This therefore gives the formula for the perihelion advance due to general relativity

$$\delta\phi_{gr} \approx \frac{6\pi GM}{c^2 A(1-e^2)} \tag{4}$$

1.4. Measurements Done on the Star S2

S2 is a star located in the star cluster near Sagittarius A* (Sgr A*), a supermassive black hole located in the center of the Milky Way. The star has an orbital period of around 16 years[11] and a mass of $13.6 \pm 0.2 M_{\odot}$ [12] whereas Sgr A* has a mass of $4.297 \times 10^6 \pm 0.012 M_{\odot}$[13].

The orbit of S2 has been observed since 1992 by the European Southern Observatory (ESO). Measurements of its velocity as well as its position relative to Sgr A* have been made by multiple instruments on ESO's Very Large Telescope (VLT). The instruments used include:

- The Nasmyth Adaptive Optics System (NAOS) - Near-Infrared Imager and Spectrograph (CONICA) or NACO[14], which contains an adaptive optics system with visible and infrared sensors as well as an infrared camera and spectrometer which together form the VLT's first adaptive optics system. By monitoring the orbits of 28 stars in the galactic center, NACO was able to provide evidence for the existence of the supermassive black hole Sgr A*.
- The Spectrograph for INtegral Field Observations in the Near Infrared or SINFONI[15] which consists of an infrared integral field spectrograph, which allows it to capture images of objects in 3 dimensions where each pixel not only represents a specific point on the object but also a full spectrum of light for that pixel which can shed light on the composition and velocity of the object. It also

contains adaptive optics which correct the disturbances in the captured images caused by the Earth's atmosphere.

- GRAVITY[16] which is an instrument on the Very Large Telescope Interferometer (VLTI) and began its observations in 2016 with position measurements with an accuracy of a few ten microarcseconds, introduced large improvements in accuracy from previous interferometric devices - it combines the light from four VLT telescopes which are each assisted by adaptive optics and also contains a fringe tracker which can provide even further corrections for disturbances caused by atmospheric turbulence.

After monitoring S2 for almost three decades, ESO's VLT detected that S2's orbit around Sgr A* was in the form of a precessing ellipse therefore suggesting that the peribothron shifts with each orbit[16]. This shift is highly aligned with the value predicted by Einstein's theory of general relativity, and it was the first measurement of such a shift occurring with a star orbiting a black hole. The detection of this shift not only allows us to better understand black holes but since the measured value aligns so closely with the value predicted by general relativity, constraints on parameters such as the amount of dark matter surrounding Sgr A* can also be found.

2. Data Analysis

2.1. Peribothron Shift

S2 has been monitored for around 27 years, which has provided us with substantial data to analyze its orbit. As previously mentioned, these measurements have been made by NACO, the near-infrared imager, and spectrograph; SINFONI, a near-infrared integral field spectrograph; and GRAVITY which is an interferometer of the VLTI which has been collecting highly accurate measurements of S2's orbit since 2016.

The data points prior to 2016 were taken from Gillesen et. al. 2016[17] which include data points from NACO and SINFONI from 1992 - 2006. For data from later years, including data from GRAVITY, we lifted the measured data points along with their associated uncertainties from GRAVITY Collaboration et. al. 2020[18]. The data set of measurements consists of the time, in years, when the measurement was taken and the right ascension and declination of S2 relative to Sgr A* along with their associated uncertainties. To be able to measure the precession of the orbit, we split the data points into two separate orbits. The time period for one complete orbit of S2 around Sgr A* has been measured to be around 16 years. Subsequently, we split the data points into those which would measure the first orbit, starting with the first measurement in 1992 and ending with the last measurement done in 2008, and the second orbit which began with the first data point in 2009 and ended with the most recent measurement done in 2019.

Plotting these points results in two ellipses that have near-identical parameters but the ellipse consisting of the second set of data points is slightly rotated which represents the peribothron shift. To model these ellipses and obtain the most accurate parameters; however, we have to take into account the uncertainties of each data point. The uncertainties in the parameters of the second ellipse are not as large as those in the first ellipse as the uncertainty in both the right ascension and declination measured by GRAVITY is only 65 microarcseconds; whereas, the uncertainty in the NACO and SINFONI data points is 0.1 milliarcseconds for the second orbit, and between 0.1 and 5 milliarcseconds for the first orbit. To take these uncertainties into account, we create a

fitting algorithm that would use a weighted total least squares approach[19] which weighs the data points based on how large their uncertainty is. The algorithm provides us with values for each coefficient in the conical equation for each of the ellipses in the form of:

$$Ax^2 + Bxy + Cy^2 + Dx + Ey = 0$$

To obtain the uncertainties of these values, we use a Monte Carlo simulation[20] which adds noise to each of the data sets and then finds the parameters using the weighted least squares method. This process is then repeated over several iterations and the standard deviation for each parameter is calculated to obtain the final uncertainty.

Thus, we obtain the parameters

Orbit 1:

	Parameter	**Uncertainty**
A	-0.955792	0.006136
B	-0.068113	0.025819
C	-0.281758	0.018084
D	-0.020449	0.003521
E	0.044891	0.004354
F	8.72×10^{-6}	2.50×10^{-4}

Orbit 2:

	Parameter	**Uncertainty**
A	-0.952861273	1.80×10^{-4}
B	-0.072235762	0.001118489
C	-0.290118225	5.19×10^{-4}
D	-0.021552909	5.03×10^{-5}
E	0.046946135	4.19×10^{-5}
F	5.80×10^{-4}	8.41×10^{-7}

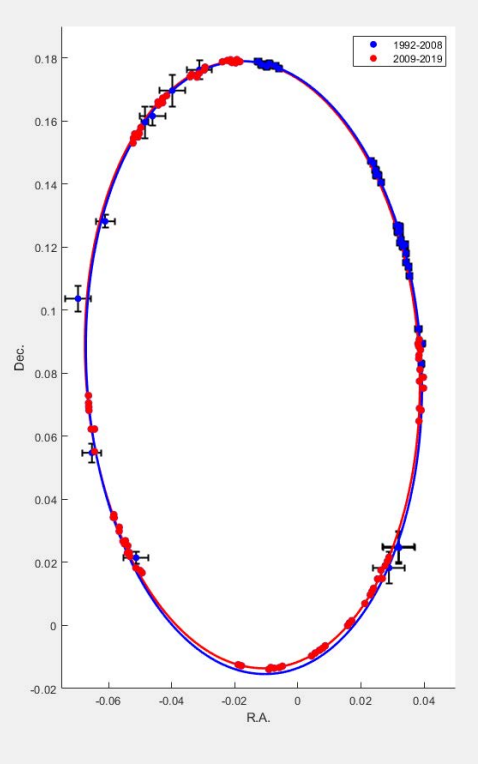

Figure 2*: The plot of the fitted orbit of S2 from 1992 - 2019. The blue data points are data points taken between 1992 and 2008 while the red data points are those taken between 2009 and 2019. Similarly, the blue ellipse represents the orbit of S2 from 1992-2008 while the red ellipse represents its orbit from 2009-2019. Although the two ellipses look very similar in shape and size, the red ellipse seems to be slightly more rotated which is an indication of the peribothron shift of S2.*

We then create another algorithm to find the semi-major axis of the ellipse and its eccentricity as well as the peribothron shift which we measure by the difference in the angle of rotation between the two ellipses. This shows that the ellipse has a semi-major axis (A) of 0.0964 ± 0.0001 arcsec and an eccentricity (e) of 0.8356 ± 0.0006. We convert the measurement for the semi-major axis from arcseconds to meters using the formula:

$$length = \frac{distance}{206265}$$

where length is the length is meters, distance is the distance from Earth to S2, which is $8.0 \pm 0.4\ kpc$[21], and θ is the value in arcseconds. This shows that the length of the semi-major axis in meters is $1.15 \times 10^{14} \pm 6 \times 10^{12} m$.

We measure the peribothron shift of S2 to be 0.0039 ± 0.0190 radians which equates to roughly 13.5 arcminutes per orbit. From this value, we subtract the peribothron shift caused by general relativistic effects, which can be found using the formula (*equation 4*):

$$\delta_g \approx \frac{6\pi G M_{BH}}{c^2 A(1-e^2)}$$

where M_{BH} is the mass of Sag A*.

Thus, we obtain that the peribothron shift not brought on by general relativistic effects is $0.00047 \pm 0.01898\, rad$.

3. Calculations

3.1. Solving for the Classical Newtonian Orbit

Our further work in sections 3.2 and 3.3 builds on the work in Wells, 'When Effective Theories Predict: The Inevitability of Mercury's Anomalous Perihelion Precession'[22]. For the sake of understanding, section 3.1 reiterates the initial steps taken in that work for section 3.2 onwards to build upon. Credit for this section goes to James D. Wells. To find the solution for the classical Newtonian orbit where the system of S2 and Sgr A* is presumed to be ideal, we first find the equations of motion using the Lagrangian. The Lagrangian for S2 following Newton's theory of gravity is:

$$L = \frac{1}{2}m\left(r'^2 + r^2\phi'^2\right) + \frac{GM_{BH}m}{r} \tag{5}$$

where $\frac{1}{2}(r^2 + r'^2\phi'^2)$ is the term for the kinetic energy in polar coordinates and $-\frac{GM_{BH}m}{r}$ is the term for the gravitational potential, with G being the gravitational constant and m being the mass of S2.

From the Lagrangian, we use the Euler-Lagrange equations for polar coordinates to obtain the radial and angular equations of motion.

To obtain the angular equation the Euler-Lagrange equation is:

$$\frac{\partial L}{\partial \phi} - \frac{d}{dt}\left(\frac{\partial L}{\partial \phi'}\right) = 0 \tag{6}$$

From these, we get that the angular equation for a classical Newtonian orbit is:

$$\frac{d}{dt}(mr^2\phi') = 0 \tag{7}$$

This shows that $mr^2\phi'$ is a constant. The angular momentum in polar coordinates is defined as $\vec{l} = \vec{r}m(r'\hat{r} + r\phi'\hat{\phi})$ and since $\vec{r} = r\hat{r}$ and the cross product $\hat{r}\hat{r} = 0$, this becomes: $\vec{l} = m\phi\phi r2(\hat{r}\hat{\phi})$ and since $\hat{r}\hat{\phi}$ is perpendicular to the motion its magnitude is equal to 1 meaning that:

$$l = mr^2\phi'$$

The angular equation derived above thus shows that the angular momentum is a constant with respect to time and it will be the same value at any point in the orbit. It can therefore also be rearranged into the form $\phi' = \frac{l}{mr^2}$

To obtain the radial equation we use the Euler-Lagrange equation:

$$\frac{\partial L}{\partial r} - \frac{d}{dt}\left(\frac{\partial L}{\partial r'}\right) = 0 \tag{8}$$

From this, we get that the radial equation for the classical Newtonian orbit is:

$$m\phi'^2 r - \frac{GM_{BH}m}{r^2} = mr'' \tag{9}$$

To find the solution to this r is substituted with $\frac{1}{u}$ and $\frac{d}{dt}$ is replaced with $\phi'\frac{d}{d\phi}$.

The equation can then be rewritten as:

$$\frac{d^2u}{d\phi^2} + u = \frac{GM_{BH}m^2}{l^2} \tag{10}$$

The solution to this equation is:

$$u(\phi) = Ccos(\phi) + \frac{GM_{BH}m^2}{l^2} \tag{11}$$

Since the equation for a classical Newtonian orbit in polar coordinates is in the form $r(\phi) = \frac{\pi}{(1 + ecos\phi)}$ [23] where p is known as the semi-latus rectum and e is the eccentricity, p is therefore equal to $\frac{l^2}{GM_{BH}m^2}$ and e is equal to Cp. From this, it can also be deduced that when e is not equal to 1, $p = a|1 - e^2|$

3.2. Equations of Motion For Orbit With a Correction to the Central Potential

To find the equations of motion for the orbit of S2 around Sgr A* with the additional gravitational effect of dark matter, we first find the Lagrangian of the star, taking into account that a mass of dark matter is also affecting the orbit of the star so a correction to the term for the potential must be introduced. The potential for dark matter if it followed the Plummer profile is (*equation 1*):

$$V_p = -\frac{GM_{DM}m}{\sqrt{(r^2 + a^2)}}$$

where M_{DM} is the mass of dark matter and a is the radius of the central core of dark matter.

Including the term for Plummer potential into the Lagrangian, we get;

$$L = \frac{1}{2}m(r'^2 + r^2\phi^2) + \frac{GM_{BH}m}{r} + \frac{GM_{DM}m}{\sqrt{(r^2 + a^2)}} \tag{12}$$

Using the same process as to obtain the equations of motion for the classical

Newtonian orbit we obtain the angular equation (7):

$$\frac{d}{dt}(mr^2\phi') = 0$$

which once again shows that the angular momentum is a constant in time, and the radial equation:

$$mr\phi^{'} - \frac{GM_{BH}m}{r^2} - \frac{GM_{DM}r}{(a^2+r^2)^{\frac{3}{2}}} = mr^{''} \tag{13}$$

As previously, we substitute $\frac{l}{mr^2}$ for ϕ', let $r = \frac{1}{u}$ as well as $\alpha = GM_{BH}m$ and replace $\frac{d}{dt}$ with $\phi'\frac{d}{d\phi}$. Similarly to the Newtonian orbit, we obtain:

$$\frac{\alpha m}{l^2}(1 + \frac{M_{DM}}{M_{BH}(a^2u^2+1)^{\frac{3}{2}}}) = \frac{d^2u}{d\phi^2} + u \tag{14}$$

We treat $\frac{\alpha m}{l^2}(1 + \frac{M_{DM}}{M_{BH}(a^2u^2+1)^{\frac{3}{2}}})$ as a small perturbation to the orbit and ignore it to first solve $\frac{\alpha m}{l^2} = \frac{d^2u}{d\phi^2} + u$, for which the solution is the formula for a standard Newtonian orbit: $\frac{1}{p}(1 + ecos\phi)$ where e is the eccentricity and $p = \frac{l^2}{GM_{BH}m^2}$. To solve for the term that causes the orbit of S2 to deviate from the standard Newtonian orbit, we substitute $\frac{1}{p}(1 + ecos\phi) + \delta u(\phi)$ into u as the orbit can now be split into the regular Newtonian orbit and the term causing it to deviate from this path, making the equation easier to solve. Since $\delta u(\phi)$ is small, any terms that are above the first order for $\delta u(\phi)$ can be ignored. We thus get the equation:

$$\frac{d^2\delta u}{d\phi^2} + \delta u = \frac{M_{DM}}{M_{BH}p} - \frac{M_{DM}3a^2}{M_{BH}2p^3}(1 + 2ecos\phi + e^2cos^2\phi) \tag{15}$$

The solution for δu is therefore:

$$\delta u = \frac{M_{DM}}{M_{BH}p} - \frac{M_{DM}3a^2}{M_{BH}2p^3}(1 + e\phi sin\phi + \frac{e^2}{3}cos2\phi + e^2sin^2\phi) \tag{16}$$

3.3. Estimating Dark Matter Density in Galactic Center

Since the peribothron shift occurs when the distance r is minimized, the peribothron can be found by solving $\frac{du}{d\phi} = 0$. This gives the equation:

$$\frac{du}{d\phi} = \frac{-esin\phi}{p} - \frac{M_{DM}a^2}{2M_{DM}p^3}(esin\phi + e\phi cos\phi - \frac{2e^2}{3}sin2\phi + 2e^2 sin\phi cos\phi) \quad (17)$$

Since the peribothron shift is the advance of the orbit beyond a complete revolution, we substitute $2\pi + \delta$ into ϕ. Assuming δ is small, $sin(\delta) \approx \delta$ and $cos(\delta) \approx 1$:

$$-e\delta - \frac{3M_{DM}a^2}{2M_{BH}p^2}(2e\delta + 2\pi e + \frac{2e^2}{3}\delta) = 0 \quad (18)$$

We then rearrange to solve for $M_{DM}a^2$ to get:

$$M_{DM}a^2 = -\frac{\delta(2M_{BH}p^2)}{6(\delta + \pi + \frac{e}{3}\delta)} \quad (19)$$

Substituting in the previously measured values:

$$M_{DM}a^2 = 5.22 \times 10^{59} \pm 2.20 \times 10^{61} kgm^2 = 2.75 \times 10^{-4} \pm 0.0116 M_{\odot}pc^2$$

All values obtained during this paper are assumed to be normally distributed and their uncertainties are assumed to be one standard deviation. Thus, we can state that the value of $M_{DM}a^2$ has a confidence level of 68%.

The formula for the Plummer density in terms of $M_{DM}a^2$ is:

$$\rho(r) = \frac{3M_{DM}a^2}{4\pi a^5}(1 + \frac{r^2}{a^2})^{\frac{-5}{2}} \quad (20)$$

Substituting in the value for $M_{DM}a^2$ in $M_{\odot}pc^2$, this becomes:

$$\rho = \frac{3(2.75 \times 10^{-4})}{4\pi a^5}(1 + \frac{r^2}{a^2})^{\frac{-5}{2}}$$

Taking a to be $0.1kpc$ [24], We get that the density of dark matter when $r = 0$, or at the galactic center, is $6.56 \times 10^{-15} M_{\odot}/pc^3$.

To obtain the upper bound of the dark matter density in the Milky Way Galactic Center, the highest value of $M_{DM}a^2$ is substituted into the equation. Thus, the equation for the upper bound of dark matter density is:

$$\rho = \frac{3(2.75 \times 10^{-4} + 0.0116)}{4\pi a^5}(1 + \frac{r^2}{a^2})^{\frac{-5}{2}} \quad (21)$$

From this, we are able to obtain that the upper bound of the density of dark matter in the Milky Way galactic center is $2.83 \times 10^{-13} M_{\odot}/pc^3$.

4. Experimental Reach

4.1. Measured S2 Orbital Data

The high precision of the observational data of S2's orbit is crucial to analyzing the properties of the galactic center. While the data from NACO and SIMFONI is on the milliarcsecond scale, data from GRAVITY is on an unprecedented macroarcsecond scale. This high precision in the measurements means that the data is not only sensitive to the contributions to the peribothron shift from the relativistic effects of Sgr A*, but is also sensitive to those caused by any dark matter present in the galactic center. This means that by studying the perturbation of S2's orbit and how much it deviates from the orbit predicted by general relativity, constraints can be put on the properties of dark matter.

However, while the gathered data is incredibly sensitive, a challenge arises due to the relatively small contribution that dark matter would make to the total peribothron shift. Due to the dominant contribution to the gravitational pull of Sgr A*, the dark matter's influence on the perturbation of the orbit would likely be minor. This can be seen in the value of the peribothron shift due to dark matter in this paper being $0.000472 \pm 0.0190 rad$, which is significantly small compared to the shift due to general relativistic effects, which is measured to be $0.0035 \pm 0.0002\ rad$. The GRAVITY collaboration also found similar results with the measured orbit being perfectly consistent with that predicted by general relativity. They introduced a dimensionless parameter that measures the strength of relativistic corrections, fSP, which equals 1 for the orbit predicted by general relativity. Their fit yielded a value of $fSP = 1.10 \pm 0.19$ which signifies a strong alignment of the orbit of S2 with that predicted by general relativity.

4.2. Orbital Fit and Measured Peribothron Shift

The observed peribothron shift was measured to be $\approx 0.00393\ rad$ with an uncertainty of $\pm 0.019 rad$. This value was estimated using a fitting algorithm that analyzed the measurements done by NACO, SIMPHONI, and GRAVITY on the VLT, which denote the right ascension and declination of S2 relative to Sgr A*. Although these measurements are highly accurate for data points from later years, especially those from GRAVITY, the associated uncertainty becomes significantly larger with older measurements. Because the older measurements were used to fit orbit 1 of S2, these uncertainties would have significantly impacted the parameters of the ellipse. Furthermore, the method used to find the peribothron shift involved splitting the measured data points into two data sets which denoted two separate orbits. This means that the orbit of S2 was approximated into two ellipses instead of one precessing ellipse. These factors combined not only led to the high uncertainty for the peribothron shift but also affected the accuracy of the measurement itself. While the value for the peribothron shift is measured by GRAVITY et al. 2020 is similar to our measured value, it is slightly smaller at $\approx 0.00349 rad$. This inaccuracy in the measurement could have further propagated throughout the equations and impacted the final value of the dark matter density.

5. Experimental Comparison

In this section, we compare the findings on dark matter density in the Milky Way dark matter halo from this paper to those reported by previous studies. Our analysis yields an upper bound of a constant density of $2.83 \times 10^{-13} M_{\odot}/pc^3$ for the central core of the halo, which decreases with an increased distance from the central core, assuming a Plummer profile for the dark matter distribution.

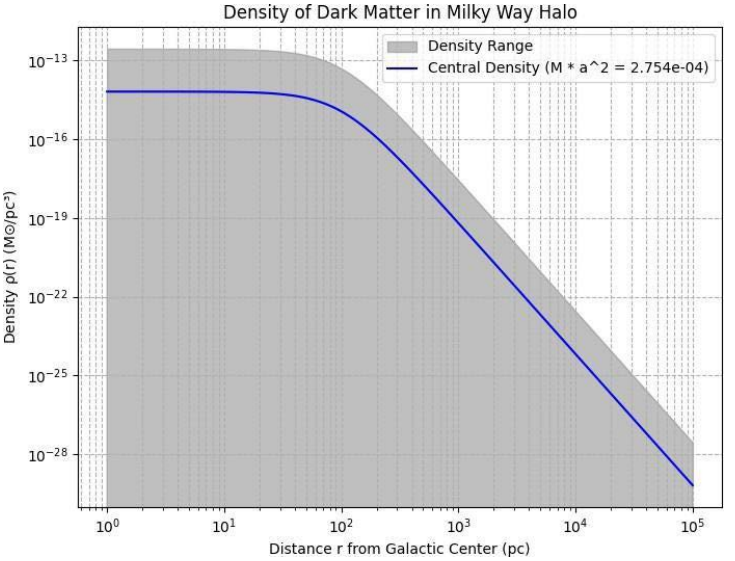

Several studies have been done on constraining the density of the Milky Way dark matter halo. For instance, Lin and Li (2019) [25] analyzed various dark matter profiles and found that for a dark matter halo that followed the Nevarro- Frenk-White (NFW) dark matter profile, the corresponding density would be $\rho = 1.34 \pm 0.24 \times 10^{-2} M_{\odot}/pc^3$, which is significantly larger than our estimated value. Other studies yield similar results such as the study done by Sofue (2011), where he analyzed the rotation curves of the Milky Way and reported a density $\rho = 7.18 \pm 0.90 \times 10^{-3} M_{\odot}/pc^3$ for the NFW profile, corroborating a higher density than our findings.

The discrepancy between our results and those from other studies could be attributed to several factors. One significant difference is the choice of the dark matter profile. While both Lin and Li (2019) and Sofue (2011) employed the NFW profile, which predicts a steeply increasing density towards the Galaxtic Center, our analysis assumes a Plummer profile. The Plummer profile is a system with a central core of a constant density which would predict a higher density in the central core which decreases with an increasing radius.

Given this, it is somewhat surprising that our derived upper bound for the core density is lower than that estimated for the NFW profile. This could be due to the nature of the data used which focused on the peribothron shift of S2 and analyzed a specific part of the galaxy, the Galactic Center, while studies that analyzed rotation curves studied larger regions of the galaxy which could potentially capture a more complete picture of the overall halo density. The data could also suggest that the dark matter is more diffused in the central core than previously thought.

However, our findings align with those of GRAVITY et al. (2019), who constrained

any extended mass inside S2's orbit to not exceed $\approx 0.1\%$ of the central mass or $\approx 4000 M_{\odot}$. The significantly lower value for the total mass of dark matter within S2's orbit that we obtained is consistent within this constraint, as it remains below the upper limit established by GRAVITY. This suggests that the dark matter contribution within the orbit of S2 is relatively minimal, which is in line with the high accordance of S2's orbit with that predicted by general relativity.

6. Discussion

6.1. Summary of Results

In this study, we analyze the peribothron shift in the orbit of the star S2 around the black hole Sgr A* to constrain dark matter density. We create a fit for the orbit S2 using data points collected over almost three decades by NACO, SIMFONI, and GRAVITY on the VLT. From this fit, we are able to find a value for the peribothron shift of S2. We assume that the Milky Way's dark matter halo follows a Plummer Profile density distribution and accordingly, introduce a correction to the potential energy term in the Lagrangian of S2. We derive the radial and angular equations of motion to ultimately find the upper bound for the dark matter density in the central core to be approximately $2.83 \times 10^{-13} M_{\odot}/pc^3$ which falls off with increased distance from the central core. This is significantly lower than other estimates for the dark matter halo; however, according to this, it is consistent with constraints on the extended mass enclosed within the orbit of S2 as it would be below the upper bound of $4000 M_{\odot}$.

6.2. Implications

Although the estimated value for the density of dark matter is significantly lower, questioning its validity, it could also imply that the dark matter is less concentrated near the Galactic Center than previously thought. A possible explanation for the lower density could be due to the dynamics of baryonic matter such as stars and dust. The Galactic Center is densely populated with stars, which can interact with dark matter through gravitational forces. These gravitational forces can cause the dark matter to be redistributed away from the central core, leading to a lower density. Furthermore, processes such as stellar feedback could additionally alter the distribution of dark matter in the galactic center. If the density of dark matter in the central core was indeed lower than previously expected, then this might have further implications on the understanding of the formation and evolution of galaxies and how dark matter interacts with galactic environments.

6.3. Further Exploration

Moving forward, there are several ways to improve and refine this study. As further measurements are done by GRAVITY, the measured orbit, and subsequently the peribothron shift, of S2 will become even more accurate, allowing for tighter constraints on the orbit's deviation from that predicted by general relativity. This would allow for even tighter constraints on the properties of dark matter in the galactic center, such as its density and mass. Furthermore, other dark matter profiles could also be explored

using the method employed in this paper. Some profiles to explore could include the Navarro-Frenk-White (NFW) profile which has been widely used in dark matter research. Analyzing this model could help improve understanding of dark matter density in relation to cusp models, where the density increases steeply with a decreased radius. Applying this method to various dark matter profiles and comparing which models best match other observational data could help constrain dark matter properties to an even greater level.

7. Appendix

7.1. Further Exploration

```
orbitdata=readmatrix('orbit1+errors.xls);
x=orbitdata(:,1);
sigma x=orbitdata(:,2);
 y=orbitdata(:,3);
sigma y=orbitdata(:4);
sigma y=orbitdata(:,4);
M = [x.^2, x.*y, y.^2, x, y, ones(length(x),1)]
 W= diag(1 ./ (sigma x.^2 + sigma y.^2));
MtW = M' *W;
[~, ~, V weighted] = svd(MtW * M, 0);
parameters = V weighted(:, end); disp(parameters);
```

7.2. Algorithm to Find Uncertainties in Ellipse Parameters

```
param distributions=zeros(num simulations,6);
M=[x.^2, x.*y, y.^2, x, y, ones(length(x), 1)];
W = diag(1 ./ (sigma x.^2 + sigma y.^2));
MtW=M'*W;
 [~, ~, V weighted] = svd(MtW * M, 0);
parameters=V weighted(:,end);
for i = 1:num simulations x noisy = x + sigma x .* randn(size(x));
y noisy = y + sigma y .* randn(size(y));
M noisy = [x noisy.^2, x noisy.*y noisy,
y noisy.^2, x noisy, y noisy, ones(length(x noisy), 1)];
W noisy = diag(1 ./ (sigma x.^2+ sigma y.^2));
 MtW noisy = M noisy' * W noisy;
[~, ~, V weighted noisy] = svd(MtW noisy * M noisy, 0); param distributions(i, :) = V
weighted noisy(:, end)'; end
param errors = std(param distributions);
```

7.3. Algorithm to Find Parameters of Orbit

```python
import numpy as np
import matplotlib.pyplot as plt
from matplotlib.patches import Ellipse

def conic_to_standard_form(A, B, C, D, E, F,sigma_A,sigma_B,sigma_C,sigma_D,sigma_E,sigma_F):
    # center of orbit
    den = B**2 - 4*A*C
    h = (2*C*D - B*E) / den
    k = (2*A*E - B*D) / den

    # shifting cetner to origin
    F_shifted = F + A*h**2 + B*h*k + C*k**2 + D*h + E*k

    # rotation angle
    theta = 0.5 * np.arctan2(B, A - C)
    cos_t = np.cos(theta)
    sin_t = np.sin(theta)

    # rotating to align with axis
    A_prime = A*cos_t**2 + B*cos_t*sin_t + C*sin_t**2
    C_prime = A*sin_t**2 - B*cos_t*sin_t + C*cos_t**2


    # semi-major and semi-minor axis
    a_squared = -F_shifted / max(A_prime, C_prime)
    b_squared = -F_shifted / min(A_prime, C_prime)

    if a_squared <= 0 or b_squared <= 0:
        raise ValueError("The given equation does not represent a valid ellipse.")

    a = np.sqrt(a_squared)
    b = np.sqrt(b_squared)

    # is semi major longer than semi minor
    if a < b:
        a, b = b, a

    sigma_h, sigma_k, sigma_theta, sigma_a, sigma_b = calculate_uncertainties(A, B, C, D, E, F, sigma_A,
     sigma_B, sigma_C, sigma_D, sigma_E, sigma_F, h, k, theta, F_shifted, A_prime, C_prime)

    print(f"Standard form: ((x - {h:.15f})^2 / {a_squared:.15f}) + ((y - {k:.15f})^2 / {b_squared:.15f}) = 1")
    print(f"Semi-major axis (a): {a:.15f} ± {sigma_a:.15f}")
    print(f"Semi-minor axis (b): {b:.15f} ± {sigma_b:.15f}")
    print(f"Center (h, k): ({h:.15f} ± {sigma_h:.15f}, {k:.15f} ± {sigma_k:.15f})")
    print(f"Rotation angle (theta): {theta:.15f} ± {sigma_theta:.15f} radians")

    return h, k, a, b, theta, sigma_h, sigma_k, sigma_theta, sigma_a, sigma_b
```

Figure 4: *Algorithm 1/3*

```
def calculate_uncertainties(A, B, C, D, E, F, sigma_A, sigma_B, sigma_C, sigma_D, sigma_E, sigma_F, h, k,
 theta, F_shifted, A_prime, C_prime):

    den = B**2 - 4*A*C


    # finding uncertaitny in each perameter for h
    dh_dA=((4*C)*(2*C*D-B*E))/den**2
    dh_dB=((E*den)-(2*B)*(2*C*D-B*E))/den**2
    dh_dC=((2*D)*den-(2*C*D-B*E)*(-4*A))/den**2
    dh_dD=((2*C*den)/den**2)
    dh_dE=(-B*den/den**2)
    dh_dF=0

    #fingind uncertainty in each parameter for k
    dk_dA=((2*A*den)-(-4*C*(2*A*E-B*D)))/den**2
    dk_dB=((-D*den)-(2*B)*(2*A*E-B*D))/den**2
    dk_dC=(-(-4*A)*(2*A*E-B*D))/den**2
    dk_dD=((-B)*den)/den**2
    dk_dE=(2*A*den)/den**2
    dk_dF=0

    #applying uncertainty for h
    sigma_h = np.sqrt((dh_dA * sigma_A)**2 +
                      (dh_dB * sigma_B)**2 +
                      (dh_dC * sigma_C)**2 +
                      (dh_dD * sigma_D)**2 +
                      (dh_dE * sigma_E)**2 +
                      (dh_dF * sigma_F))


    #applying uncertainty for k
    sigma_k = np.sqrt((dk_dA * sigma_A)**2 +
                      (dk_dB * sigma_B)**2 +
                      (dk_dD * sigma_D)**2 +
                      (dk_dE * sigma_E)**2 +
                      (dk_dF * sigma_F))


    # uncertainty for rotation angle
    dtheta_dA = 0.5 * (B**2 / (A - C)**2) / (1 + (B / (A - C))**2)
    dtheta_dB = 0.5 / (A - C) / (1 + (B / (A - C))**2)
    dtheta_dC = -0.5 * (B**2 / (A - C)**2) / (1 + (B / (A - C))**2)
```

Figure 5: *Algorithm 2/3*

```
    dF_shifted_dA=h**2
    dF_shifted_dB=h*k
    dF_shifted_dC=k**2
    dF_shifted_dD=h
    dF_shifted_dE=k
    dF_shifted_dF=1

    sigma_F_shifted = np.sqrt((dF_shifted_dA * sigma_A)**2 +
                              (dF_shifted_dB * sigma_B)**2 +
                              (dF_shifted_dC * sigma_C)**2 +
                              (dF_shifted_dD * sigma_D)**2 +
                              (dF_shifted_dE * sigma_E)**2 +
                              (dF_shifted_dF * sigma_F)**2)

    cos_t = np.cos(theta)
    sin_t = np.sin(theta)
    sigma_A_prime = np.sqrt((cos_t**2 * sigma_A)**2 + (cos_t*sin_t * sigma_B)**2 + (sin_t**2 * sigma_C)**2)
    sigma_C_prime = np.sqrt((sin_t**2 * sigma_A)**2 + (cos_t*sin_t * sigma_B)**2 + (cos_t**2 * sigma_C)**2)

    sigma_a_squared = np.sqrt((sigma_F_shifted / max(A_prime, C_prime))**2 +
                              (F_shifted * sigma_A_prime / max(A_prime, C_prime)**2)**2)

    sigma_b_squared = np.sqrt((sigma_F_shifted / min(A_prime, C_prime))**2 +
                              (F_shifted * sigma_C_prime / min(A_prime, C_prime)**2)**2)

    a_squared = -F_shifted / max(A_prime, C_prime)
    b_squared = -F_shifted / min(A_prime, C_prime)

    sigma_a = sigma_a_squared / (2 * np.sqrt(a_squared))
    sigma_b = sigma_b_squared / (2 * np.sqrt(b_squared))

    return sigma_h, sigma_k,sigma_theta,sigma_a,sigma_b

h, k, a, b, theta, sigma_h, sigma_k, sigma_theta, sigma_a, sigma_b = conic_to_standard_form(A, B, C, D, E, F,
sigma_A, sigma_B, sigma_C, sigma_D, sigma_E, sigma_F)
```

Figure 6: *Algorithm 3/3*

7.4. Data Set for Orbit 1:

R.A.	ΔR.A.	Dec	ΔDec.
-0.0060	1.0000e-03	0.1766	1.0000e-03
-0.0072	1.0000e-03	0.1776	1.0000e-03
-0.0091	1.0000e-03	0.1782	1.0000e-03
-0.0099	1.0000e-03	0.1773	1.0000e-03
-0.0115	1.0000e-03	0.1779	1.0000e-03
-0.0126	1.0000e-03	0.1789	1.0000e-03
-0.0313	0.0040	0.1762	0.0030
-0.0461	0.0040	0.1616	0.0030
-0.0485	1.0000e-03	0.1596	0.0050
-0.0612	0.0030	0.1282	0.0020
-0.0653	0.0030	0.0548	0.0030
-0.0513	0.0040	0.0215	0.0020
0.0394	1.0000e-03	0.0894	1.0000e-03
0.0382	1.0000e-03	0.0941	1.0000e-03
0.0391	1.0000e-03	0.0829	1.0000e-03

0.0354	1.0000e-03	0.1109	1.0000e-03
0.0351	1.0000e-03	0.1137	1.0000e-03
0.0343	1.0000e-03	0.1152	1.0000e-03
0.0342	1.0000e-03	0.1180	1.0000e-03
0.0333	1.0000e-03	0.1202	1.0000e-03
0.0340	1.0000e-03	0.1208	1.0000e-03
0.0324	1.0000e-03	0.1214	1.0000e-03
0.0326	1.0000e-03	0.1225	1.0000e-03
0.0313	1.0000e-03	0.1269	1.0000e-03
0.0322	1.0000e-03	0.1266	1.0000e-03
0.0317	1.0000e-03	0.1248	1.0000e-03
0.0323	1.0000e-03	0.1250	1.0000e-03
0.0263	1.0000e-03	0.1406	1.0000e-03
0.0255	1.0000e-03	0.1428	1.0000e-03
0.0248	1.0000e-03	0.1428	1.0000e-03
0.0246	1.0000e-03	0.1445	1.0000e-03
0.0239	1.0000e-03	0.1466	1.0000e-03
0.0231	1.0000e-03	0.1473	1.0000e-03

7.5. Data Set for Orbit 2:

R.A.	**ΔR.A.**	**Dec**	**ΔDec.**
-0.0184	1.0000e-03	0.1788	1.0000e-03
-0.0193	1.0000e-03	0.1795	1.0000e-03
-0.0198	1.0000e-03	0.1784	1.0000e-03
-0.0210	1.0000e-03	0.1786	1.0000e-03
-0.0214	1.0000e-03	0.1794	1.0000e-03
-0.0224	1.0000e-03	0.1792	1.0000e-03
-0.0240	1.0000e-03	0.1788	1.0000e-03
-0.0294	1.0000e-03	0.1771	1.0000e-03
-0.0298	1.0000e-03	0.1762	1.0000e-03
-0.0313	1.0000e-03	0.1752	1.0000e-03
-0.0320	1.0000e-03	0.1739	1.0000e-03
-0.0337	1.0000e-03	0.1748	1.0000e-03
-0.0342	1.0000e-03	0.1740	1.0000e-03
-0.0417	1.0000e-03	0.1681	1.0000e-03
-0.0429	1.0000e-03	0.1673	1.0000e-03
-0.0429	1.0000e-03	0.1658	1.0000e-03
-0.0444	1.0000e-03	0.1660	1.0000e-03
-0.0443	1.0000e-03	0.1651	1.0000e-03

-0.0498	1.0000e-03	0.1580	1.0000e-03
-0.0503	1.0000e-03	0.1560	1.0000e-03
-0.0508	1.0000e-03	0.1549	1.0000e-03
-0.0518	1.0000e-03	0.1559	1.0000e-03
-0.0522	1.0000e-03	0.1546	1.0000e-03
-0.0523	1.0000e-03	0.1530	1.0000e-03
-0.0665	1.0000e-03	0.0729	1.0000e-03
-0.0664	1.0000e-03	0.0706	1.0000e-03
-0.0664	1.0000e-03	0.0693	1.0000e-03
-0.0663	1.0000e-03	0.0682	1.0000e-03
-0.0645	1.0000e-03	0.0623	1.0000e-03
-0.0656	1.0000e-03	0.0623	1.0000e-03
-0.0494	1.0000e-03	0.0167	1.0000e-03
-0.0501	1.0000e-03	0.0174	1.0000e-03
-0.0540	1.0000e-03	0.0253	1.0000e-03
-0.0547	1.0000e-03	0.0269	1.0000e-03
-0.0567	1.0000e-03	0.0312	1.0000e-03
-0.0585	1.0000e-03	0.0343	1.0000e-03
0.0213	1.0000e-03	0.0070	1.0000e-03
0.0253	1.0000e-03	0.0147	1.0000e-03
0.0268	1.0000e-03	0.0149	1.0000e-03
0.0264	1.0000e-03	0.0175	1.0000e-03
0.0391	1.0000e-03	0.0683	1.0000e-03

R.A.	**ΔR.A.**	**Dec**	**ΔDec.**
0.0399	1.0000e-03	0.0753	1.0000e-03
0.0398	1.0000e-03	0.0787	1.0000e-03
0.0389	1.0000e-03	0.0874	1.0000e-03
0.0385	1.0000e-03	0.0907	1.0000e-03
-0.0645	6.5000e-05	0.0551	6.5000e-05
-0.0584	6.5000e-05	0.0351	6.5000e-05
-0.0583	6.5000e-05	0.0342	6.5000e-05
-0.0567	6.5000e-05	0.0299	6.5000e-05
-0.0555	6.5000e-05	0.0267	6.5000e-05
-0.0550	6.5000e-05	0.0259	6.5000e-05
-0.0541	6.5000e-05	0.0230	6.5000e-05
-0.0535	6.5000e-05	0.0231	6.5000e-05
-0.0533	6.5000e-05	0.0219	6.5000e-05
-0.0514	6.5000e-05	0.0183	6.5000e-05
-0.0190	6.5000e-05	-0.0125	6.5000e-05
-0.0179	6.5000e-05	-0.0128	6.5000e-05
-0.0092	6.5000e-05	-0.0139	6.5000e-05

-0.0086	6.5000e-05	-0.0133	6.5000e-05
-0.0076	6.5000e-05	-0.0136	6.5000e-05
-0.0059	6.5000e-05	-0.0133	6.5000e-05
-0.0050	6.5000e-05	-0.0129	6.5000e-05
0.0043	6.5000e-05	-0.0097	6.5000e-05
0.0055	6.5000e-05	-0.0087	6.5000e-05
0.0069	6.5000e-05	-0.0078	6.5000e-05
0.0079	6.5000e-05	-0.0072	6.5000e-05
0.0087	6.5000e-05	-0.0065	6.5000e-05
0.0158	6.5000e-05	-2.9866e-05	6.5000e-05
0.0164	6.5000e-05	7.9567e-04	6.5000e-05
0.0171	6.5000e-05	0.0015	6.5000e-05
0.0230	6.5000e-05	0.0097	6.5000e-05
0.0235	6.5000e-05	0.0108	6.5000e-05
0.0240	6.5000e-05	0.0118	6.5000e-05
0.0277	6.5000e-05	0.0190	6.5000e-05
0.0284	6.5000e-05	0.0204	6.5000e-05
0.0289	6.5000e-05	0.0217	6.5000e-05
0.0384	6.5000e-05	0.0648	6.5000e-05
0.0386	6.5000e-05	0.0689	6.5000e-05
0.0386	6.5000e-05	0.0775	6.5000e-05
0.0388	6.5000e-05	0.0812	6.5000e-05
0.0384	6.5000e-05	0.0846	6.5000e-05
0.0384	6.5000e-05	0.0857	6.5000e-05
0.0383	6.5000e-05	0.0885	6.5000e-05
0.0381	6.5000e-05	0.0894	6.5000e-05

References

[1] Martin White. Rotational curves, Oct 2014.

[2] Yoshiaki Sofue, Y Tutui, M Honma, A Tomita, T Takamiya, J Koda, and Y Takeda. Central rotation curves of spiral galaxies. *The Astrophysical Journal*, 523(1):136, 1999.

[3] Julio F Navarro. The structure of cold dark matter halos. In *Symposium- international astronomical union*, volume 171, pages 255–258. Cambridge University Press, 1996.

[4] H. C. Plummer. On the problem of distribution in globular star clusters: (plate 8.). *Monthly Notices of the Royal Astronomical Society*, 71(5):460–470, Mar 1911.

[5] Chang Chen, Yin Li, Francisco Villaescusa-Navarro, Shirley Ho, and Anthony Pullen. Learning the evolution of the universe in n-body simulations. *arXiv preprint arXiv:2012.05472*, 2020.

[6] Herwig Dejonghe. A completely analytical family of anisotropic plummer models.

Monthly Notices of the Royal Astronomical Society, 224(1):13–39, 1987.

[7] WJG De Blok. The core-cusp problem. *Advances in Astronomy*, 2010(1):789293, 2010.

[8] Roger A Rydin. Le verrier's 1859 paper on mercury, and possible reasons for mercury's anomalous precession. *The General Science Journal (Dec 22, 2009)*, 2009.

[9] Galina Weinstein. Einstein, schwarzschild, the perihelion motion of mercury and the rotating disk story. *arXiv preprint arXiv:1411.7370*, 2014.

[10] Christian Corda. The secret of planets' perihelion between newton and einstein. *Physics of the dark universe*, 32:100834, 2021.

[11] A Boehle, AM Ghez, R Sch¨odel, L Meyer, S Yelda, S Albers, GD Martinez, EE Becklin, T Do, JR Lu, et al. An improved distance and mass estimate for sgr a* from a multistar orbit analysis. *The Astrophysical Journal*, 830(1):17, 2016.

[12] M Habibi, S Gillessen, Fabrice Martins, F Eisenhauer, PM Plewa, O Pfuhl, E George, J Dexter, I Waisberg, T Ott, et al. Twelve years of spectroscopic monitoring in the galactic center: The closest look at s-stars near the black hole. *The Astrophysical Journal*, 847(2):120, 2017.

[13] R Abuter, N Aimar, P Amaro Seoane, A Amorim, M Baub¨ock, JP Berger, H Bonnet, G Bourdarot, W Brandner, V Cardoso, et al. Polarimetry and astrometry of nir flares as event horizon scale, dynamical probes for the mass of sgr a. *Astronomy & Astrophysics*, 677:L10, 2023.

[14] Rainer Lenzen, Markus Hartung, Wolfgang Brandner, Gert Finger, Norbert N Hubin, Francois Lacombe, Anne-Marie Lagrange, Matthew D Lehnert, Alan FM Moorwood, and David Mouillet. Naosconica first on-sky results in a variety of observing modes. In *Instrument Design and Performance for Optical/Infrared Ground-based Telescopes*, volume 4841, pages 944–952. SPIE, 2003.

[15] Frank Eisenhauer, Roberto Abuter, Klaus Bickert, Fabio Biancat-Marchet, Henri Bonnet, Joar Brynnel, Ralf D Conzelmann, Bernard Delabre, Robert Donaldson, Jacopo Farinato, et al. Sinfoni: integral field spectroscopy at 50-milli-arcsecond resolution with the eso vlt. In *Instrument Design and Performance for Optical/ Infrared Ground-based Telescopes*, volume 4841, pages 1548–1561. SPIE, 2003.

[16] Roberto Abuter, Matteo Accardo, A Amorim, N Anugu, Gerardo Avila, N Azouaoui, Myriam Benisty, Jean-Philippe Berger, Nicolas Blind, Henri Bonnet, et al. First light for gravity: Phase referencing optical interferometry for the very large telescope interferometer. *Astronomy & Astrophysics*, 602:A94, 2017.

[17] Stefan Gillessen, PM Plewa, Frank Eisenhauer, Re'em Sari, Idel Waisberg, Maryam Habibi, Oliver Pfuhl, Elizabeth George, Jason Dexter, Sebastiano von Fellenberg, et al. An update on monitoring stellar orbits in the galactic center. *The Astrophysical Journal*, 837(1):30, 2017.

[18] R Abuter, A Amorim, M Baub¨ock, JP Berger, H Bonnet, W Brandner, V Cardoso, Y Cl´enet, PT De Zeeuw, J Dexter, et al. Detection of the schwarzschild precession in the orbit of the star s2 near the galactic centre massive black hole. *Astronomy & Astrophysics*, 636:L5, 2020.

[19] A Amiri-Simkooei and S Jazaeri. Weighted total least squares formulated by standard least squares theory. *Journal of geodetic science*, 2(2):113–124, 2012.

[20] Samik Raychaudhuri. Introduction to monte carlo simulation. In *2008 Winter simulation conference*, pages 91–100. IEEE, 2008.

[21] F Eisenhauer, R Sch¨odel, R Genzel, T Ott, M Tecza, R Abuter, A Eckart, and Tal Alexander. A geometric determination of the distance to the galactic center. *The Astrophysical Journal*, 597(2):L121, 2003.

[22] James D Wells. When effective theories predict: the inevitability of mercury's anomalous perihelion precession. *arXiv preprint arXiv:1106.1568*, 2011.

[23] Department of Applied Mathematics Cambridge University and Theoretical Physics. *Chapter 8 Orbits 8.1 Conics*. Cambridge University, Feb 2012.

[24] Lorenzo Posti and Amina Helmi. Mass and shape of the milky way's dark matter halo with globular clusters from gaia and hubble. *Astronomy & Astrophysics*, 621:A56, 2019

[25] Hai-Nan Lin and Xin Li. The dark matter profiles in the milky way. *Monthly Notices of the Royal Astronomical Society*, 487(4):5679–5684, 201

Publisher
Pioneer Academics, PBC
101 Greenwood Avenue, Ste. 170
Jenkintown, PA 19046

ISSN 2996-1971

Pioneer Academics, PBC
Email: info@pioneeracademics.com
Website: www.pioneeracademics.com

The Pioneer Research Journal is published annually by Pioneer Academics, PBC. The 2024 issue of *The Pioneer Research Journal* is Volume 11.